Physics of the Dark Universe 46 (2024) 101646

Contents lists available at ScienceDirect

Physics of the Dark Universe

journal homepage: www.elsevier.com/locate/dark

Finch–Skea quintessence models in non-conservative theory of gravity

M.R. Shahzad [a,1], Asifa Ashraf [b,*,1], M. Awais Qarni [a], Emad E. Mahmoud [c], Wen-Xiu Ma [b,d,e,f,*]

[a] Department of Mathematics, Bahauddin Zakariya University, Vehari Campus, Vehari 61100, Pakistan
[b] School of Mathematical Sciences, Zhejiang Normal University, Jinhua, Zhejiang 321004, China
[c] Department of Mathematics and Statistics, College of Science, Taif University, P.O. Box 11099, Taif 21944, Saudi Arabia
[d] Department of Mathematics, King Abdulaziz University, Jeddah 21589, Saudi Arabia
[e] Department of Mathematics and Statistics, University of South Florida, Tampa, FL 33620-5700, USA
[f] School of Mathematical and Statistical Sciences, North-West University, Mafikeng Campus, Private Bag X2046, Mmabatho 2735, South Africa

ARTICLE INFO

Keywords:
Quintessence field
Compact stars
Finch–Skea geometry
Stability
Rastall theory of gravity

ABSTRACT

This study is dedicated to presenting a new solution of the field equations in the Rastall theory with a quintessence field defined by the parameter ω_q as $-1 < \omega_q < -\frac{1}{3}$ by considering the isotropic matter content inside the sphere. The Finch–Skea ansatz (FS) is used in a static and spherically symmetric geometry to obtain the feasible relativistic solution. The results obtained in the physical evaluation are analyzed analytically and graphically. In the appropriate limit of the Rastall coupling parameter, one can regain the original results in the General Relativity. This complete analysis considers five different compact stars: $HerX-1$ with mass $0.88M_{\odot}$ and radius 7.7 km, $VelaX-12$ with mass $1.77M_{\odot}$ and radius 9.99 km, $SAXJ1808-3658(SSI)$ with mass $1.435M_{\odot}$ and radius 7.07 km, $4U1608-52$ with mass $1.74M_{\odot}$ and radius 9.30 km, $4U1538-52$ with mass $0.87M_{\odot}$ and radius 7.86 km and $PSRJ1416-2230$ with mass $1.97M_{\odot}$ and radius 10.30 km. The physical validity of the obtained solution is verified by computing the necessary physical parameters like energy density and pressure, quintessence density, energy conditions, sound speed via the Herrera cracking concept, hydrostatic equilibrium of forces, mass function, compactness, Buchdahl limit, and surface redshift and analyze their behavior graphically. To investigate the demeanor of these parameters more closely, we computed the numerical values and manifested them in tabular form. We conclude that our presented mathematical model of compact stars in the Finch–Skea geometry with quintessence field fulfills all the requirements for a physically viable solution.

1. Introduction

The general theory of relativity (GR) has been beneficial for explaining gravitational dynamics in the current era. But in the 1920s, Edwin Hubble's innovative observations revealed that our universe is not static rather it is accelerating which makes the GR stagnant to explain such phenomena and opens the door for the researcher's community to discover modified theories of GR to deal with such phenomena [1–11]. 68 percent of the universe is made up of Dark Energy (DE), which is the pivotal factor in the expansion of the universe. Over time, many modified theories have been discovered to understand this expansion of the universe and to explain many other mysterious features of the universe that remain consistent with the observational data. A part of them, in 1972, Rastall [12] also suggested a modified theory by modifying the conservation law of energy–momentum tensor represented (EMT) as $\nabla_b \mathbb{T}^b_a \propto \mathbb{R}_{,a}$ by using a dimensionless parameter called Rastall parameter. In this modification, the covariant divergence of the EMT does not vanish but remains directly proportional to the gradient of the scalar curvature. Moreover, in exception, by keeping the value of the Rastall parameter equal to zero, the GR can be restored.

In modern astrophysics, the advancements in cosmology, more precise observations, and simulations have led us to the fascinating realm of celestial objects with such unusual properties, extremes of density and gravity, and behaviors that challenge our current knowledge of physics [13,14]. The development of these highly dense celestial objects is the result of supernova [15]. Based on compactness, compact objects are classified into different classes, including white dwarfs, neutron stars, and black holes. Several authors have proposed the models of stellar structures to understand their interior structure and celestial properties in different modified theories of gravity. In this regime Maurya et al. [16–22] proposed several models of stellar structures and

* Corresponding authors.
E-mail addresses: dr.rizwanshahzad@bzu.edu.pk (M.R. Shahzad), asifamustafa3828@gmail.com (A. Ashraf), aq187530@gmail.com (M.A. Qarni), e.Mahmoud@tu.edu.sa (E.E. Mahmoud), wma3@usf.edu (W.-X. Ma).
[1] First two authors have equal contribution.

https://doi.org/10.1016/j.dark.2024.101646
Received 19 July 2024; Received in revised form 4 September 2024; Accepted 7 September 2024
Available online 12 September 2024

discussed their interior properties which are compatible with the observational studies. Mustafa and his collaborators [23–28] investigated the structure of compact objects in different modified gravity theories.

Several studies in astrophysics have also been carried out recently by using different metric potentials and in different scenarios in the realm of RT [29–31]. Saleem et al. [32] studied the implications of the RT by considering the generic form of the metric potential functions. Majeed and Abbas [33] proposed a gravastar model in the RT and discussed its properties by taking into account the Tolman–Kuchowicz solution. Moradpour and Salako [34] analyze the constraints of RT by applying the Newtonian limit on GR and further in [35], showed the better role of RT than GR by observing the comparison of thermodynamics quantities like entropy and energy in both RT and GR counterpart. Fabris et al. [36] also studied the characteristics of the celestial models in the realm of RT. Darabi et al. [37] oppose Visser's claim [38] by contrasting the RT with GR and explaining their difference by considering the example of the well-studied $f(R)$ gravity theory.

Later, Hansraj et al. [39] also considered the same dispute as Darabi et al. [37] and the results are again in favor of Darabi et al. [37] study. In this study, they presented the comparative analysis of the RT and GR to challenge Visser's claim. They showed that RT adequately fulfills the necessary basic requirements for a viable stellar model in most of the cases, while the gGR model shows deviations from these conditions. Indeed, experimental evidence has been shown against the Visser's claim. Hansraj and Banerjee [40] later replicated their earlier findings to challenge Visar's claim. They studied physical parameters for modeling stellar structures in RT and GR. Again, they observed that the RT model seemed to fit with these constraints, while the GR model violated some basic constraints. Empirical results support the results of Darabi et al. (2018) to dispute Visser's claim. As a result of the present discussion, Shahzad along with his collaborators [41–50] have delved into this debate and propounded several relativistic stellar models by employing various techniques. These investigations also support the nonequivalence of these two theories. Recently, marvelous achievement made by Nashed [51] also opposed the speculation of the Visser's claim. Furthermore, in [52–58] some perceptual results of astronomy have been studied including inflation problems and rapid expansion of the universe. To check the accuracy, limits, and boundaries of gravitational theory, a solar system test(SST) is applied to it and observe whether it illustrates the interior structure of stellar objects or not. Recently, [59] conducted the SST in the realm of RT by considering a celestial body as a neutral regular Hayward black hole to study the relativistic effect. In [60], some vigorous black hole solutions have been observed and compared with GR. A novel BH solution has been proposed in the Rastall framework when applying to nonlinear electrodynamics [61]. Recently Nashed and El Hanafy [62] proposed a new class of stellar structure in the RT consistent with the observational outcomes. Moreover, El Hanafy [63–65] further investigated the implications of the RT on the mass and radius of Pulsars. Afshar et al. [66] studied the primary inflationary and reheating eras in the RT concluding that the outcomes are well consistent with the observational data as compared to the GR. Dayanandan et al. [67] investigated the Finch–Skea geometry to develop reliable relativistic anisotropic models of the stellar objects by utilizing the class one solution.

Motivated by the recent interesting consequences of RT, this manuscript explores some new solutions of field equations by using Finch–Skea geometry in the framework of RT for an isotropic matter content in a static and symmetrical symmetric geometry. The sequence of the study is as follows: the next section deals with the formation of the field equation and corresponding new solution in the RT. In Section 3, we present matching conditions to determine the values of the unknown constants involved, Section 4 deals with the physical analysis of the obtained model to check the physical plausibility. In the last section, we present a brief summary and conclude our findings.

2. Rastall field equations and their solution

By assuming Finch–Skea geometry [68], the spherically symmetric line-element for a static geometry is represented as;

$$ds^2 = -e^{\phi(r)}dt^2 + e^{\psi(r)}dr^2 + r^2d\theta^2 + r^2\sin^2\theta d\varphi^2, \tag{1}$$

where metric potentials ψ and ϕ are differentiable and functions of r, the radial coordinate, such that $\psi(r) = cr^2 + 1$ and $\phi(r) = \left(A + \frac{1}{2}Br\sqrt{cr^2}\right)^2$ [68], where A, B, c are constants determined by matching conditions. Several authors have successfully employed the Finch–Skea ansatz to study the well-behaved stellar structures in different modified gravity theories [69–76]. The energy–momentum tensor (EMT) $\mathfrak{T}_{\lambda\nu}$ representing the isotropic matter distribution is

$$\mathfrak{T}_{\lambda\nu} = (p+\rho)\xi_\lambda\xi_\nu + pg_{\lambda\nu}, \tag{2}$$

where p and ρ are pressure and energy density respectively. Moreover, ξ^a representing the four-velocity satisfying the constraints $\xi^\lambda = e^{-\frac{\phi}{2}}\delta^\lambda_0$, $\xi^\lambda\xi_\lambda = -1$.

Rastall's amendment [77] for energy–momentum conservation law is given as;

$$\nabla_\nu\mathfrak{T}^\nu_\lambda = \alpha\mathfrak{R}_{,\lambda}, \tag{3}$$

where α is the Rastall parameter, the deflection of Rastall's theory from standard GR, and shows the combination of matter field with configuration. The modification, for acquiring field equations, is given as ;

$$G_{\lambda\nu} + \alpha\kappa g_{\lambda\nu}\mathfrak{R} = \kappa\mathfrak{T}_{\lambda\nu}, \tag{4}$$

here κ is gravitational coupling constant of RT. The trace of Eq. (4) yield, $\mathfrak{R}(4\alpha\kappa - 1) = \mathfrak{T}$, where $\mathfrak{T}$ is the trace of the EMT, from which one can observe that T will become zero for $\alpha\kappa = \frac{1}{4}$ that is not allowed because $\mathfrak{T}$ may not be always zero. Also the equations for α and κ, by using Newtonian limit and Rastall dimensionless parameter $\gamma = \alpha\kappa$, can be represented as [78]

$$\kappa = \left(\frac{4-\frac{1}{\gamma}}{6-\frac{1}{\gamma}}\right)8\pi, \tag{5}$$

$$\alpha = \left(\frac{4-\frac{1}{\gamma}}{6-\frac{1}{\gamma}}\right)\frac{\gamma}{8\pi}, \tag{6}$$

from Eqs. (5) and (6) one can observe that for $\gamma = \frac{1}{6}$ and $\gamma = \frac{1}{4}$, both κ and α will become undefined, so these two values are not acceptable for physical solutions in the RT. So the Rastall's field equations can be obtained as;

$$G_{\lambda\nu} + \gamma g_{\lambda\nu}\mathfrak{R} = 8\pi\mathfrak{T}_{\lambda\nu}\left(\frac{4-\frac{1}{\gamma}}{6-\frac{1}{\gamma}}\right), \tag{7}$$

And also in terms of the quintessence field, Eq. (7) becomes;

$$G_{\lambda\nu} + \gamma g_{\lambda\nu}\mathfrak{R} = 8\pi(\tau_{\lambda\nu} + \mathfrak{T}_{\lambda\nu})\left(\frac{4-\frac{1}{\gamma}}{6-\frac{1}{\gamma}}\right), \tag{8}$$

where $\tau_{\lambda\nu}$ is the EMT for quintessence field, suggested by Kiselev [79] that should satisfy the conditions of linearity and additivity. Thus $\tau_{\lambda\nu}$ in component form read as;

$$\tau^t_t = \tau^r_r = \rho_q, \tag{9}$$

$$\tau^\theta_\theta = \tau^\phi_\phi = \frac{3\omega_q + 1}{2}\rho_q, \tag{10}$$

here ω_q is the quintessence parameter constrained as $-1 < \omega_q < -\frac{1}{3}$, and equations. (1), (2) and (7) ;

$$8\pi(\rho+\rho_q)\left(\frac{1-4\gamma}{1-6\gamma}\right) = e^{-\psi}\left[\frac{e^\psi - 1}{r^2} + \frac{\psi'}{r} + \gamma\left\{\phi'' - \psi'\phi' + \phi'^2\right.\right.$$

Table 1
Estimated values of A and B.

Compact star	$M(M_\odot)$	R (km)	c (km^{-2})	A	B (km^{-1})
$SAXJ1808.4-3658(SSI)$	1.435	7.07	0.01424235696	0.46323821878	0.03994212933
$VelaX-12$	1.77	9.99	0.01097191713	0.50175825917	0.03618423648
$HerX-1$	0.88	7.7	0.00857852402	0.71063568642	0.03770389876
$PSRJ1614-2230$	1.97	10.3	0.01220429124	0.44645623624	0.03646349459
$4U1608-52$	1.74	9.3	0.01424235696	0.46323821878	0.03994212933
$4U1538-52$	0.87	7.86	0.00784789636	0.72118270739	0.03635020124

$$+\frac{2}{r}(\psi'-\frac{e^{\psi}}{r^2}+\frac{1}{r}-\phi')\Big\}\Big], \tag{11}$$

$$8\pi(p-\rho_q)\left(\frac{1-4\gamma}{1-6\gamma}\right)=e^{-\psi}\left[\frac{1-e^{\psi}}{r^2}+\frac{\phi'}{r}-\gamma\left\{\phi''-\psi'\phi'+\phi'^2+\frac{2}{r}(\psi'-\frac{e^{\psi}}{r^2}+\frac{1}{r}-\phi')\right\}\right], \tag{12}$$

$$4\pi(2p+(3\omega_q+1)\rho_q)\left(\frac{1-4\gamma}{1-6\gamma}\right)=e^{-\psi}\left[(\phi'-\psi')(\frac{\psi'}{4}+\frac{1}{2r})+\frac{\phi''}{2}-\gamma\left\{\phi''-\psi'\phi'+\phi'^2+\frac{2}{r}(\psi'-\frac{e^{\psi}}{r^2}+\frac{1}{r}-\phi')\right\}\right]. \tag{13}$$

By assuming Finch Skea symmetry [68] the equation. (11) to (13) can be solved and involved material variables can be manipulated as (see Table 1),

$$\begin{aligned}\rho=&-\frac{1}{24\pi(4\gamma-1)(\omega_q+1)\sqrt{cr^2}(cr^2+1)^2(2A+Br\sqrt{cr^2})^2}\\&\times\Big[c(6\gamma-1)(4A^2\sqrt{cr^2}(cr^2(6\gamma(\omega_q+1)\\&-3\omega_q-1)+9(2\gamma-1)(\omega_q+1)))+4ABr(6\gamma(\omega_q+1)(cr^2-1)(cr^2+3)\\&-cr^2(cr^2(3\omega_q+1)+9\omega_q+11))\\&+B^2r^2\sqrt{cr^2}(6\gamma(\omega_q+1)(cr^2-5)(cr^2+2)\\&-cr^2(cr^2(3\omega_q+1)+9\omega_q+13))\Big]\end{aligned}$$

$$\begin{aligned}p=&\frac{1}{24\pi(4\gamma-1)(\omega_q+1)\sqrt{cr^2}(cr^2+1)^2(2A+Br\sqrt{cr^2})^2}\\&\times\Big[c(6\gamma-1)(4A^2\sqrt{cr^2}(cr^2(6\gamma(\omega_q+1)\\&-3\omega_q-1)+3(6\gamma-1)(\omega_q+1))+4ABr(c^2r^4(6\gamma(\omega_q+1)-3\omega_q-1)\\&+cr^2(12\gamma(\omega_q+1)+3\omega_q+1)-6(3\gamma-1)(\omega_q+1))\\&+B^2r^2\sqrt{cr^2}(c^2r^4(6\gamma(\omega_q+1)-3\omega_q-1)\\&+cr^2(-18\gamma(\omega_q+1)+9\omega_q+5)-12(5\gamma-1)(\omega_q+1)))\Big]\end{aligned}$$

$$\rho_q=\frac{c(6\gamma-1)r\left(4A^2cr+4AB\left(cr^2-1\right)\sqrt{cr^2}+B^2cr^3\left(cr^2-2\right)\right)}{12\pi(4\gamma-1)(\omega_q+1)\left(cr^2+1\right)^2\left(2A+Br\sqrt{cr^2}\right)^2} \tag{14}$$

3. Matching conditions

The constants (A, B, c) involved in Finch Skea metric potential and appearing in the above expressions can be obtained by using matching conditions at the boundary. So the corresponding exterior Schwarzschild metric is,

$$ds^2=-W\,dt^2+\frac{1}{W}dr^2+r^2(d\theta^2+\sin^2\theta d\phi^2), \tag{15}$$

Table 2
Calculated values of matter variables for $4U1538-52$ in the RT. In the following Tables 2–7, ρ_0, ρ_s, p_0 represent the central density, surface density, and central pressure, respectively.

γ	Mass from our model (km)	$\frac{2M}{R}$	Z_s	ρ_0 gm (cm)$^{-3}$ $\times10^{13}$	ρ_s gm (cm)$^{-3}$ $\times10^{13}$	p_0 dyn (cm)$^{-2}$
0	1.22790	$0.31244<\frac{8}{9}$	0.20599	5.81143	5.14750	1.13761×10^{36}
0.01	1.19121	$0.30310<\frac{8}{9}$	0.19789	6.75733	5.62500	1.10430×10^{36}
0.02	1.15282	$0.29333<\frac{8}{9}$	0.18958	7.64334	6.06612	1.02258×10^{36}
0.03	1.11248	$0.28307<\frac{8}{9}$	0.18103	8.46132	6.46592	1.03263×10^{36}
0.04	1.06991	$0.27224<\frac{8}{9}$	0.17221	9.20152	6.81848	9.93775×10^{35}

Table 3
Calculated values of matter variables for $(VelaX-12)$ in the RT.

γ	Mass from our model (km)	$\frac{2M}{R}$	Z_s	ρ_0 gm (cm)$^{-3}$ $\times10^{13}$	ρ_s gm (cm)$^{-3}$ $\times10^{13}$	p_0 dyn (cm)$^{-2}$
0	2.41301	$0.48308<\frac{8}{9}$	0.39088	2.22037	8.16456	1.59046×10^{36}
0.01	2.34534	$0.46953<\frac{8}{9}$	0.37300	2.28193	8.38188	1.54762×10^{36}
0.02	2.27411	$0.45527<\frac{8}{9}$	0.35491	2.33447	8.56648	1.50235×10^{36}
0.03	2.19882	$0.44020<\frac{8}{9}$	0.33655	2.37678	8.71392	1.45431×10^{36}
0.04	2.11890	$0.42420<\frac{8}{9}$	0.31785	2.39052	8.76133	1.43424×10^{36}

Table 4
Calculated values of matter variables for $4U1608-52$ in the RT.

γ	Mass from our model (km)	$\frac{2M}{R}$	Z_s	ρ_0 gm (cm)$^{-3}$ $\times10^{14}$	ρ_s gm (cm)$^{-3}$ $\times10^{14}$	p_0 dyn (cm)$^{-2}$
0	2.35967	$0.50745<\frac{8}{9}$	0.42487	3.40261	1.05055	2.06454×10^{36}
0.01	2.29481	$0.49350<\frac{8}{9}$	0.40512	3.45639	1.07161	2.01031×10^{36}
0.02	2.22640	$0.47879<\frac{8}{9}$	0.38514	3.49823	1.08878	1.95285×10^{36}
0.03	2.15396	$0.46321<\frac{8}{9}$	0.36490	3.52652	1.10153	1.89174×10^{36}
0.04	2.07691	$0.44664<\frac{8}{9}$	0.34431	3.53931	1.10923	1.82645×10^{36}

here $W=\frac{r-2M}{r}$ and M is the mass of the star. Now by comparing the coefficient of Eqs. (1) and (15), we get the values of unknowns (A, B, c),

$$A=\frac{2R-5M}{2\sqrt{R}\sqrt{R-2M}} \tag{16}$$

$$B=\frac{\sqrt{M}}{\sqrt{2}R^{\frac{3}{2}}} \tag{17}$$

$$c=\frac{2M}{R^2(R-2M)}. \tag{18}$$

4. Some physical features of the proposed model

This section deals with the physical plausibility of our proposed model. To do so, we evaluate some mathematical consequences and check their physical essence, arithmetically as well as graphically. Also, their numerical values are given in tabular form (see Fig. 3).

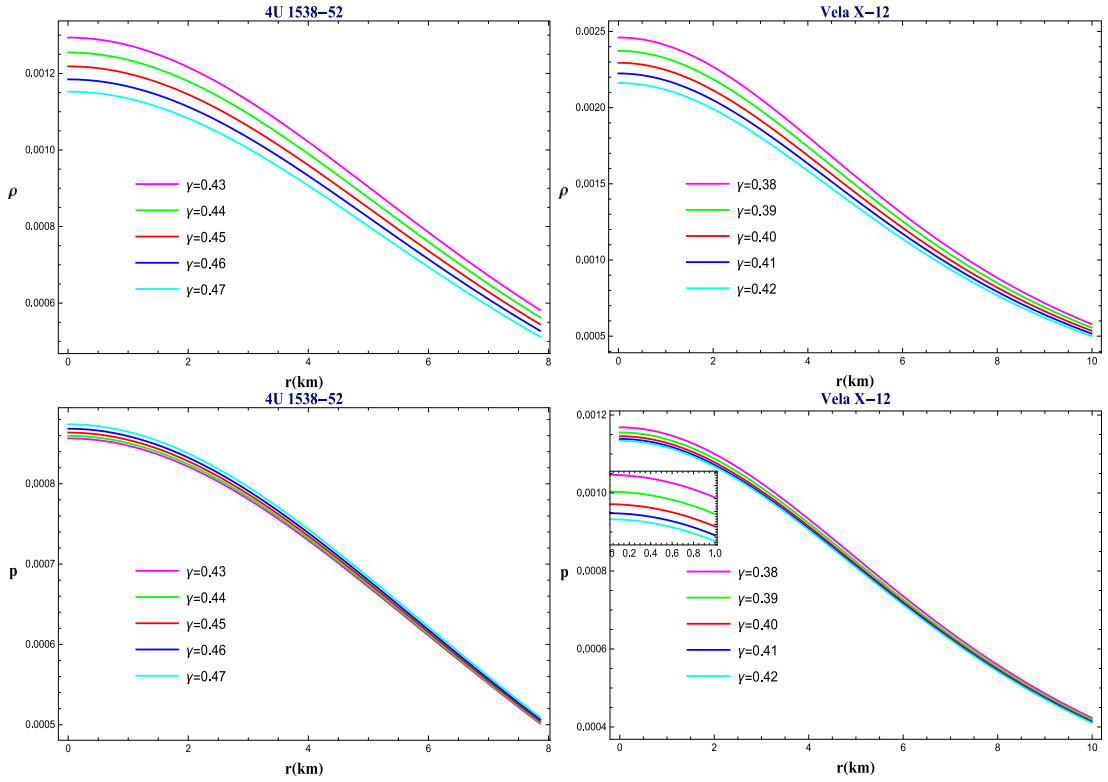

Fig. 1. Profile of the energy density describing the distribution of energy density along the radial coordinate with various values of γ for two different stars indicated in the left and right panels of the first row (i.e., first panel for $4U1538-52$ and second for Vela X-12). The second row features the conduct of pressure along the radial coordinate.

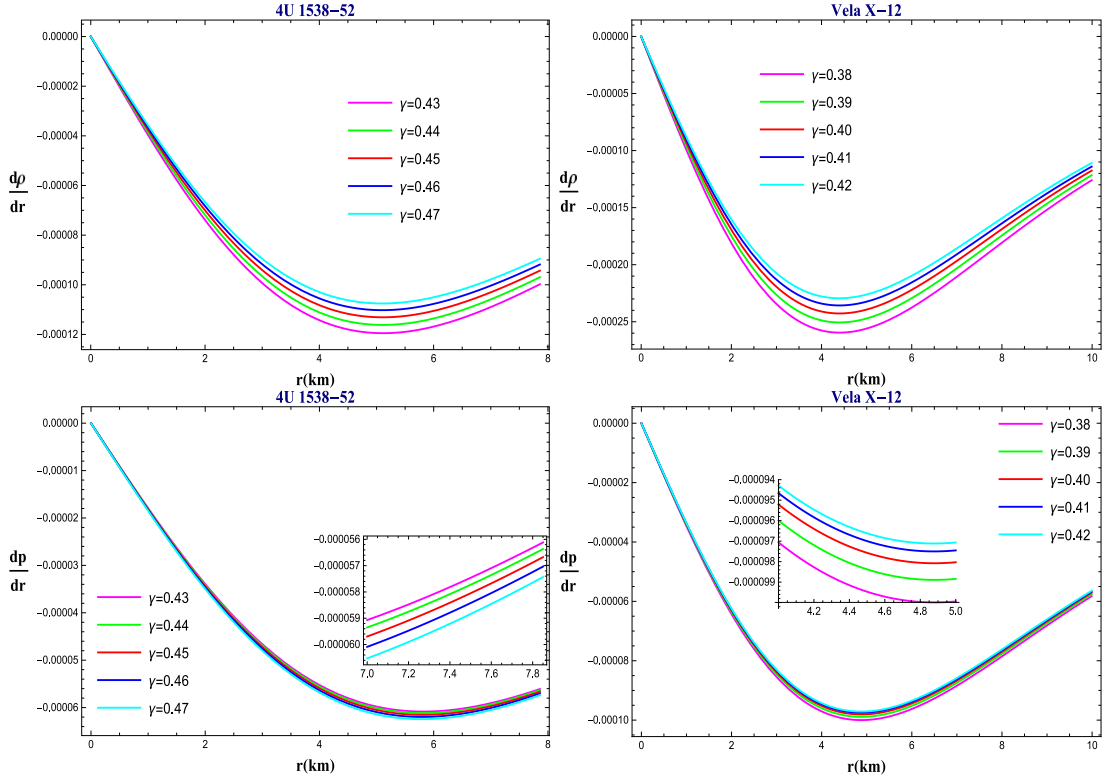

Fig. 2. Behavior of the radial derivative of energy density describing the influence of γ on the optimal criterion of the energy density (first row), which is indicated at the center. The trend of the radial derivative of pressure is indicated in the second row for various values of γ and a small portion is magnified to clearly observe the different curves.

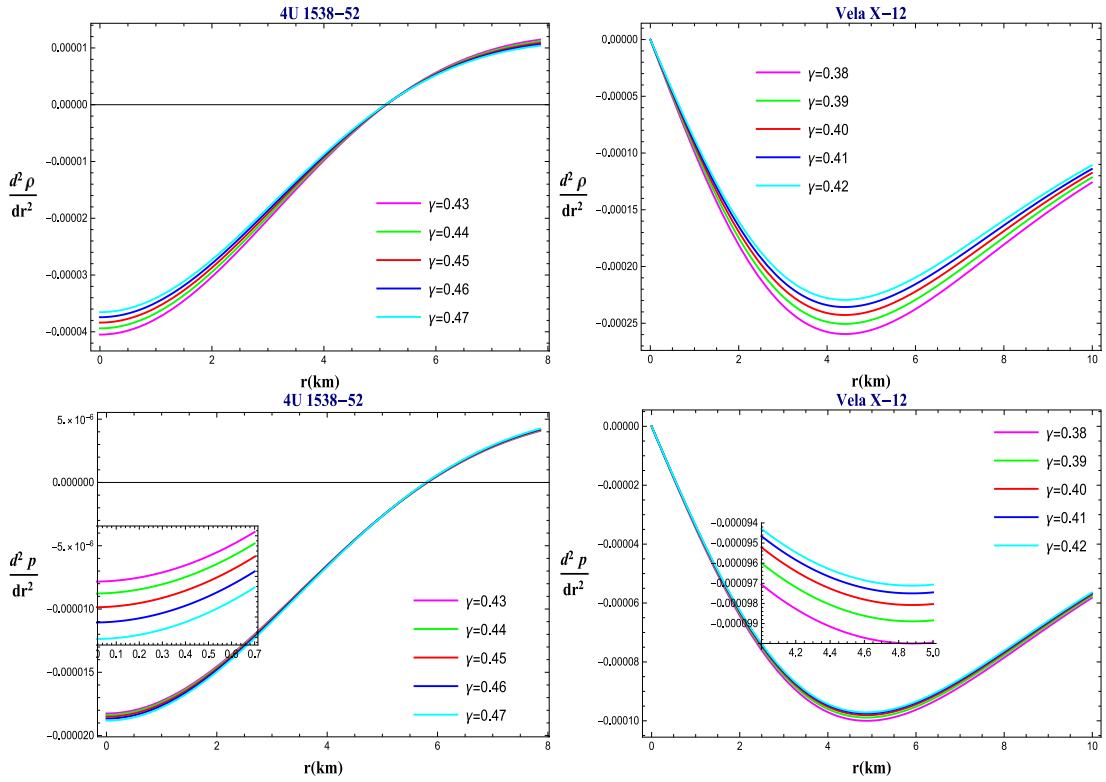

Fig. 3. Double derivative of energy density along the radial coordinate to confirm whether the optimal point is maxima (or minima) by using the double derivative test (first row), which indicates that the density is maximum at the core of the star. The second line represents the graphical conduct of the double derivative of pressure to confirm the maximal point (the point at which the pressure is maximum) for different chosen values of γ.

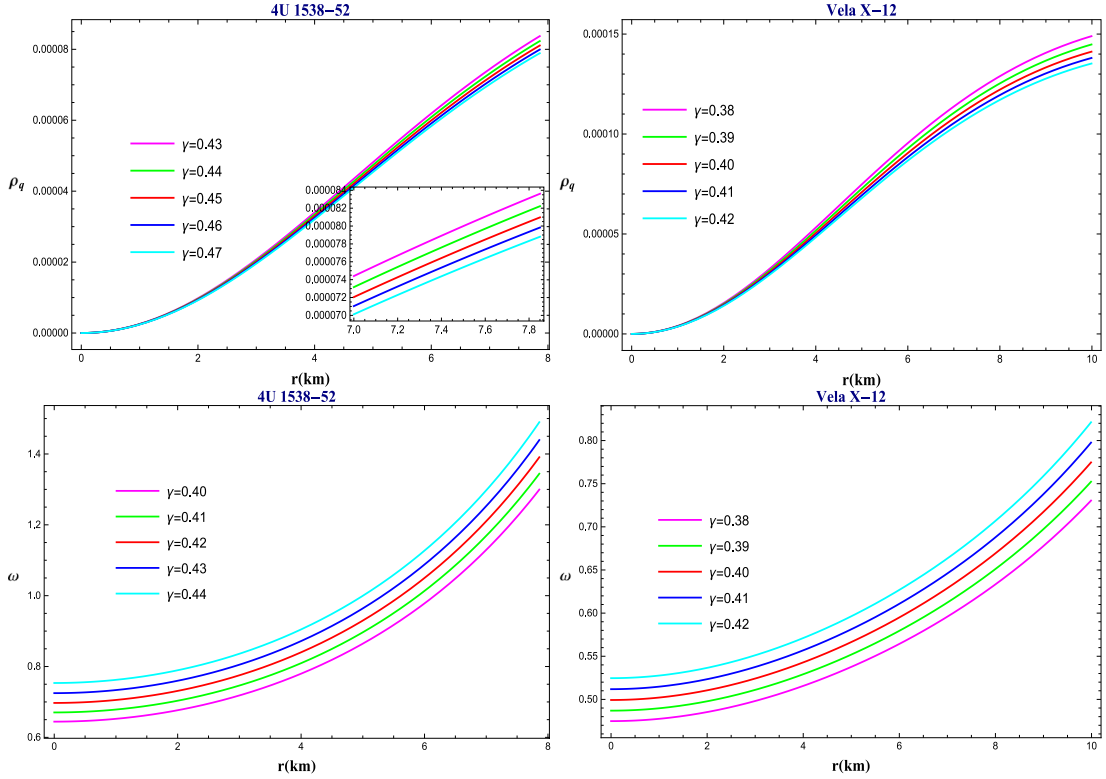

Fig. 4. Graphical behavior of quintessence energy density ρ_q (appeared due to the quintessence field) along the radial coordinate (first row) and the range of the equation of state parameter EoS parameter ω_q is represented in the second row for considered two different stars. In both cases (i.e. for both considered stats) the ω_q remains in the stable region (0,1).

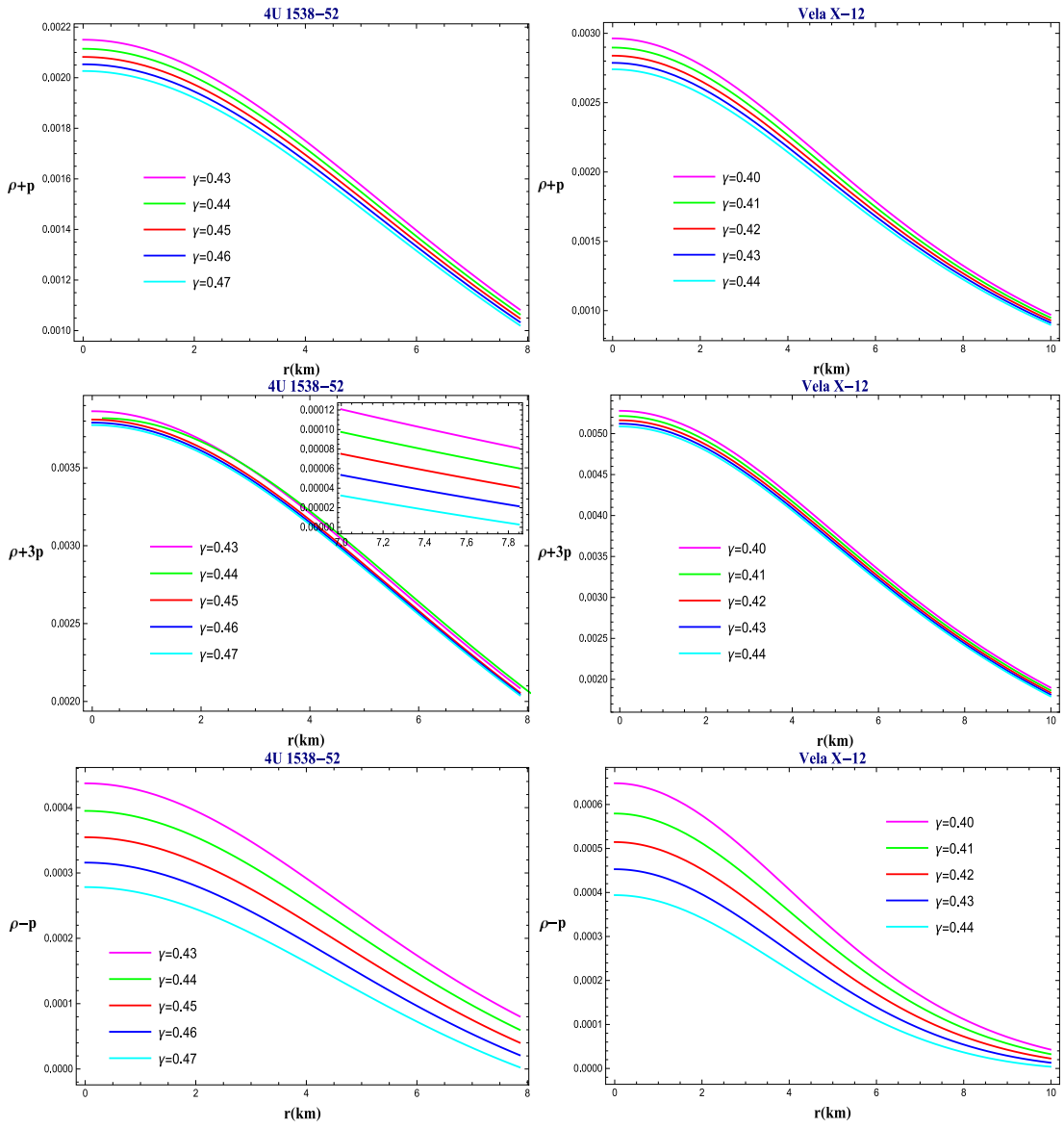

Fig. 5. Graphical conduct of the energy conditions represented by inequalities given in Eq. (25) along the radial coordinate for the considered stars in this study, for different values of the Rastall parameter. In all the cases (i.e. for both stars and all chosen values of γ), the inequalities Eq. (25) holds good.

Table 5
Calculated values of matter variables for $SAX1808.4-3658(SS1)$ in the RT.

γ	Mass from our model (km)	$\frac{2M}{R}$	Z_s	ρ_0 gm (cm)$^{-3}$ $\times 10^{14}$	ρ_s gm (cm)$^{-3}$ $\times 10^{14}$	p_0 dyn (cm)$^{-2}$
0	1.40096	$0.39631 < \frac{8}{9}$	0.28704	9.53819	2.13931	4.32767×10^{36}
0.01	1.36310	$0.38560 < \frac{8}{9}$	0.27577	9.53013	2.16126	4.22036×10^{36}
0.02	1.32310	$0.37428 < \frac{8}{9}$	0.26419	9.49597	2.17626	4.10599×10^{36}
0.03	1.28067	$0.36228 < \frac{8}{9}$	0.25223	9.43216	2.18336	3.98362×10^{36}
0.04	1.23547	$0.34949 < \frac{8}{9}$	0.23986	9.33445	2.18143	3.85209×10^{36}

Table 6
Calculated values of matter variables for $HerX-1$ in the RT.

γ	Mass from our model (km)	$\frac{2M}{R}$	Z_s	ρ_0 gm (cm)$^{-3}$ $\times 10^{13}$	ρ_s gm (cm)$^{-3}$ $\times 10^{13}$	p_0 dyn (cm)$^{-2}$
0	1.23986	$0.32204 < \frac{8}{9}$	0.21450	6.70944×10^{13}	5.71808	1.24352×10^{36}
0.01	1.20288	$0.31243 < \frac{8}{9}$	0.20599	7.72547×10^{13}	6.21816	1.20721×10^{36}
0.02	1.16418	$0.30238 < \frac{8}{9}$	0.19726	8.67589×10^{13}	6.67923	1.16913×10^{36}
0.03	1.12350	$0.29181 < \frac{8}{9}$	0.18830	9.55175×10^{13}	7.09599	1.12903×10^{36}
0.04	1.08058	$0.28067 < \frac{8}{9}$	0.17906	1.03423×10^{14}	7.46209	1.08664×10^{36}

4.1. Physical attributes of pressure and energy density

For the physical acceptance of energy density(ρ) and pressure (p), both ρ and p should remain positive within the radius and also should be monotonically decreasing as the radius increases. Moreover, it should remain singularity-free through the entire radius. To fulfill all these conditions, we check out it graphically as shown in Fig. 1 satisfying the condition (positive essence of energy density and pressure). Also, in order to check their optimal values, we also plot the gradients of density and pressure (Fig. 2) which remain negative throughout the entire layout and vanish as $r \to 0$, indicating optimal values at the core. The negative values of gradients of ρ and p are shown in Fig. 2 and Fig. 3 indicate the decreasing nature of ρ and p. The graphical representation of the quintessence energy density (ρ_q) Fig. 4 (left panel) increases as the radius increases and also it vanishes at the core. The numerical values of ρ and p at the core and surface density for different

Table 7
Calculated values of matter variables for $PSRJ1614-2230$ in the RT.

γ	Mass from our model (km)	$\frac{2M}{R}$	Z_s	ρ_0 $gm\ (cm)^{-3}$ $\times 10^{14}$	ρ_s $gm\ (cm)^{-3}$ $\times 10^{13}$	p_0 $dyn\ (cm)^{-2}$
0	2.66589	$0.51764 < \frac{8}{9}$	0.43985	3.13595	8.95018	1.76910×10^{36}
0.01	2.59334	$0.50356 < \frac{8}{9}$	0.41927	3.17097	9.10597	1.72321×10^{36}
0.02	2.51676	$0.48869 < \frac{8}{9}$	0.39848	3.19567	9.22973	1.67453×10^{36}
0.03	2.43558	$0.47292 < \frac{8}{9}$	0.37741	3.20863	9.31706	1.62269×10^{36}
0.04	2.34915	$0.45614 < \frac{8}{9}$	0.35599	3.20820	9.36278	1.56723×10^{36}

values of γ are given in Tables 2–7 and for different stars. The equations for the maximum ρ and p at the core can be acquired as:

$$\rho_0 = -\frac{(6\gamma-1)(9a(2\gamma-1)(\omega_q+1)-18B\gamma(\omega_q+1))}{24\pi(4\gamma-1)(\omega_q+1)}, \tag{19}$$

$$p_0 = \frac{(6\gamma-1)(3a(6\gamma-1)(\omega_q+1)-6B(3\gamma-1)(\omega_q+1))}{24\pi(4\gamma-1)(\omega_q+1)}, \tag{20}$$

and the derivatives of density and pressure are

$$\begin{aligned}\frac{\mathrm{d}\rho}{\mathrm{dr}} &= \frac{1}{12\pi(4\gamma-1)(\omega_q+1)\sqrt{cr^2}(cr^2+1)^3(2A+Br\sqrt{cr^2})^3}\\ &\times\Big[c(6\gamma-1)r(8A^3c\sqrt{cr^2}(cr^2(6\gamma(\omega_q+1)\\ &-3\omega_q-1)+30\gamma(\omega_q+1)-15\omega_q-17)\\ &+4A^2Bcr(3c^2r^4(6\gamma(\omega_q+1)-3\omega_q-1)\\ &+cr^2(78\gamma(\omega_q+1)-5(9\omega_q+11))-60\gamma(\omega_q+1)+4)\\ &+2AB^2\sqrt{cr^2}(6\gamma(\omega_q+1)(3cr^2(cr^2(cr^2+3)-8)-2)\\ &-cr^2(3c^2r^4(3\omega_q+1)+9cr^2(5\omega_q+7)-4))\\ &+B^3cr^3(6\gamma(\omega_q+1)(cr^2(cr^2-10)(cr^2+3)-10)\\ &-c^2r^4(cr^2(3\omega_q+1)+5(3\omega_q+5))))\Big],\end{aligned} \tag{21}$$

$$\begin{aligned}\frac{\mathrm{dp}}{\mathrm{dr}} &= -\frac{1}{12\pi(4\gamma-1)(\omega_q+1)\sqrt{cr^2}(cr^2+1)^3(2A+Br\sqrt{cr^2})^3}\\ &\times\Big[c(6\gamma-1)r(8A^3c\sqrt{cr^2}(cr^2(6\gamma(\omega_q+1)\\ &-3\omega_q-1)+30\gamma(\omega_q+1)-3\omega_q-5)+4A^2Bcr(3c^2r^4(6\gamma(\omega_q+1)\\ &-3\omega_q-1)+cr^2(78\gamma(\omega_q+1)+3\omega_q-7)\\ &+4(-15\gamma(\omega_q+1)+3\omega_q+4))\\ &+2AB^2\sqrt{cr^2}(3c^3r^6(6\gamma(\omega_q+1)-3\omega_q-1)+9c^2r^4(6\gamma(\omega_q+1)\\ &+3\omega_q+1)+4cr^2(-36\gamma(\omega_q+1)+12\omega_q+13)\\ &-12(\gamma-1)(\omega_q+1))+B^3cr^3(c^3r^6(6\gamma(\omega_q+1)\\ &-3\omega_q-1)+c^2r^4(-42\gamma(\omega_q+1)+21\omega_q+11)\\ &-36c(5\gamma-1)r^2(\omega_q+1)-12(5\gamma-1)(\omega_q+1)))\Big],\end{aligned} \tag{22}$$

$$\begin{aligned}\frac{d^2\rho}{\mathrm{dr}^2} &= -\frac{1}{12\pi(4\gamma-1)(\omega_q+1)\sqrt{cr^2}(cr^2+1)^4(2A+Br\sqrt{cr^2})^4}\\ &\times\Big[c(6\gamma-1)(16A^4c\sqrt{cr^2}(3c^2r^4(6\gamma(\omega_q+1)\\ &-3\omega_q-1)+2cr^2(66\gamma(\omega_q+1)-33\omega_q-41)\\ &-30\gamma(\omega_q+1)+15\omega_q+17)\\ &+32A^3Bcr(3c^3r^6(6\gamma(\omega_q+1)-3\omega_q-1)\\ &+c^2r^4(123\gamma(\omega_q+1)-66\omega_q-85)+cr^2(5(3\omega_q+5)\\ &-96\gamma(\omega_q+1))+15\gamma(\omega_q+1)-1)\\ &+8A^2B^2\sqrt{cr^2}(6\gamma(\omega_q+1)(cr^2(cr^2(9cr^2(cr^2+6)-94)+6)\\ &+1)+cr^2(4-cr^2(9cr^2(cr^2(3\omega_q+1)+22\omega_q+30)-45\omega_q-103)))\\ &+8AB^3cr^3(3\gamma(\omega_q+1)(cr^2(cr^2(cr^2(6cr^2+29)-94)+13)+10)\\ &+cr^2(3-cr^2(cr^2(3cr^2(3\omega_q+1)+66\omega_q+101)-15\omega_q-37)))\\ &+B^4r^2(cr^2)^{3/2}(6\gamma(\omega_q+1)\\ &\times(cr^2(cr^2(cr^2(3cr^2-38)-203)-120)-30)\\ &-c^2r^4(cr^2(3cr^2(3\omega_q+1)+66\omega_q+122)-5(3\omega_q+5))))\Big],\end{aligned} \tag{23}$$

and

$$\begin{aligned}\frac{d^2p}{\mathrm{dr}^2} &= \frac{1}{12\pi(4\gamma-1)(\omega_q+1)\sqrt{cr^2}(cr^2+1)^4(2A+Br\sqrt{cr^2})^4}\\ &\times\Big[c(6\gamma-1)(16A^4c\sqrt{cr^2}(3c^2r^4(6\gamma(\omega_q+1)\\ &-3\omega_q-1)+2cr^2(66\gamma(\omega_q+1)-3\omega_q-11)\\ &-30\gamma(\omega_q+1)+3\omega_q+5)\\ &+32A^3Bcr(3c^3r^6(6\gamma(\omega_q+1)-3\omega_q-1)\\ &+c^2r^4(123\gamma(\omega_q+1)+3\omega_q-16)+cr^2(-96\gamma(\omega_q+1)\\ &+9\omega_q+19)+15\gamma(\omega_q+1)-3\omega_q-4)\\ &+8A^2B^2\sqrt{cr^2}(9c^4r^8(6\gamma(\omega_q+1)-3\omega_q-1)\\ &+18c^3r^6(18\gamma(\omega_q+1)+3\omega_q-1)\\ &+c^2r^4(-564\gamma(\omega_q+1)+75\omega_q+133)+4cr^2(9\gamma(\omega_q+1)-3\omega_q-2)\\ &+6(\gamma-1)(\omega_q+1))+8AB^3cr^3(3c^4r^8(6\gamma(\omega_q+1)-3\omega_q-1)\\ &+c^3r^6(87\gamma(\omega_q+1)+51\omega_q+16)\\ &+c^2r^4(-282\gamma(\omega_q+1)+87\omega_q+109)\\ &+3cr^2(13\gamma(\omega_q+1)+11\omega_q+12)+6(5\gamma+1)(\omega_q+1))\\ &+B^4r^2(cr^2)^{3/2}(3c^4r^8(6\gamma(\omega_q+1)-3\omega_q-1)\\ &+2c^3r^6(-114\gamma(\omega_q+1)+57\omega_q+29)\\ &+c^2r^4(-1218\gamma(\omega_q+1)+231\omega_q+241)\\ &-144c(5\gamma-1)r^2(\omega_q+1)+36(1-5\gamma)(\omega_q+1)))\Big].\end{aligned} \tag{24}$$

In order to satisfy the non-exotic nature of our system Fig. 4 (right plot) shows that the EoS parameter $w=\frac{p}{\rho}$ is bounded within the limit, between zero to one.

4.2. Energy constraints

This section delves into the properties of physical characteristics of stellar structures, focusing on some energy conditions necessary for their stability. A stellar model is deemed viable physically when it adheres to necessary energy constraints throughout its interior. In the context of stellar modeling, these energy conditions are of paramount importance. Utilizing basic framework of GR, we can express energy conditions as local inequalities that regulate the relationship between energy density (ρ) and pressure (p), constrained by particular conditions. While there are numerous methods for establishing energy criteria, our primary focus is on the energy condition governing by the following constraints,

$$\rho \geq 0, \quad \rho + p \geq 0, \quad \rho + 3p \geq 0, \quad \rho \geq |p|. \tag{25}$$

In order to satisfy the above inequalities, we plot their graphs Fig. 5, which satisfy these inequalities and show the non-exotic nature of matter in essence which adds more value to our proposed model.

4.3. TOV equation

This study portion investigates hydrostatic equilibrium within the stellar interior due to the influence of gravitational, hydrostatic forces along with an extra force due to the modified gravity (usually called Rastall force). The Tolman–Oppenheimer–Volkoff (TOV) equation

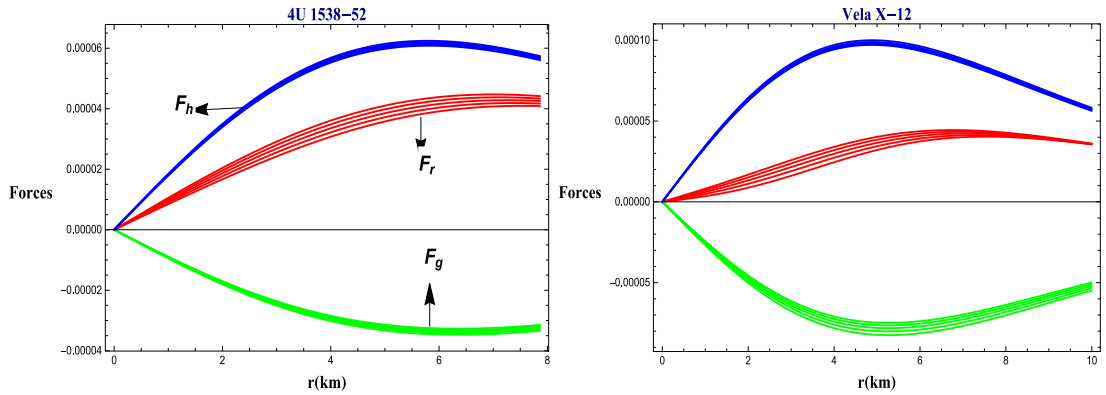

Fig. 6. Graphical evolution of forces acting on the system along the radial coordinate for various values of the Rastall parameter γ, which indicates that our model is in the hydrostatic equilibrium state. The role of the force F_r due to the RT is significant to counterbalance the net effect of the total forces.

serves as a key tool in characterizing the internal structure of the compact object. The TOV equation mathematically encapsulates the balance of these forces, ensuring that the stellar model remains in a state of equilibrium. By analyzing the contributions of gravitational, hydrostatic, and Rastall forces, we can ascertain the conditions under which a star can maintain its stability against perturbations. The TOV equation in the RT involving these forces can be stated as:

$$\left(\frac{1}{4-\frac{1}{\gamma}}\right)\frac{d}{dr}(\rho-3p)+\frac{\phi'}{2}(-\rho-p)-\frac{dp}{dr}=0, \tag{26}$$

The first, second, and third terms in the above equation respectively represent the Rastall, gravitational, and hydrostatic forces.

The equilibrium state of these forces is graphically represented in Fig. 6 which consolidates the proposed model. For $\gamma = 0$ the Rastall force will vanish and we can get the TOV equation in the GR case.

4.4. Stability analysis

Here is a way to check the stability of the proposed model which is called Stability via sound speed. We will use Herrera's cracking concept [80] to check the casualty condition. For this, the squared sound speed of the system must remain positive throughout the configuration and never exceed the limit of the speed of light, which means $0 < V_s^2 = \frac{dp}{d\rho} \leq 1$. Here V_s^2 for isotropic model is formulated as:

$$V_s^2=\frac{dp}{d\rho}=\frac{V_1}{V_2}, \tag{27}$$

which gives $V_s^2 = \frac{V_1}{V_2}$, where

$$\begin{aligned}V_1 =\ & -(8A^3c\sqrt{cr^2}(cr^2(6\gamma(\omega_q+1)-3\omega_q-1)\\ &+30\gamma(\omega_q+1)-3\omega_q-5)+4A^2Bcr(3c^2r^4(6\gamma(\omega_q+1)\\ &-3\omega_q-1)+cr^2(78\gamma(\omega_q+1)+3\omega_q-7)\\ &+4(-15\gamma(\omega_q+1)+3\omega_q+4))\\ &+2AB^2\sqrt{cr^2}(3c^3r^6(6\gamma(\omega_q+1)-3\omega_q-1)\\ &+9c^2r^4(6\gamma(\omega_q+1)+3\omega_q+1)+4cr^2(-36\gamma(\omega_q+1)\\ &+12\omega_q+13)-12(\gamma-1)(\omega_q+1))\\ &+B^3cr^3(c^3r^6(6\gamma(\omega_q+1)-3\omega_q-1)+c^2r^4(-42\gamma(\omega_q+1)\\ &+21\omega_q+11)-36c(5\gamma-1)r^2(\omega_q+1)-12(5\gamma-1)(\omega_q+1)),\end{aligned}$$

$$\begin{aligned}V_2 =\ & 8A^3c\sqrt{cr^2}(cr^2(6\gamma(\omega_q+1)-3\omega_q-1)+30\gamma(\omega_q+1)-15\omega_q-17)\\ &+4A^2Bcr(3c^2r^4(6\gamma(\omega_q+1)-3\omega_q-1)+cr^2(78\gamma(\omega_q+1)\\ &-5(9\omega_q+11))-60\gamma(\omega_q+1)+4)\\ &+2AB^2\sqrt{cr^2}(6\gamma(\omega_q+1)(3cr^2(cr^2(cr^2+3)-8)-2)\\ &-cr^2(3c^2r^4(3\omega_q+1)+9cr^2(5\omega_q+7)-4))\\ &+B^3cr^3(6\gamma(\omega_q+1)(cr^2(cr^2-10)(cr^2+3)-10)-c^2r^4(cr^2(3\omega_q+1)\\ &+5(3\omega_q+5)))),\end{aligned}$$

The graphical demonstration of V_s^2 is given in Fig. 7 indicating that our proposed model fulfills the causality condition.

4.5. Mass-radius relation

Herein, we described that how the connection between the radius and mass of the stellar body influenced the viability of the proposed model. The formulation for the relativistic mass is as follows:

$$M(r)=\int_0^r 4r^2\pi\rho dr \tag{28}$$

The relation between mass and radius should be such that, as the radius approaches zero the mass of the celestial object should also approach zero and the mass $M(r)$ remains singularity-free throughout the whole configuration. For this, the physical deportment of $M(r)$ in Fig. 8 is represented showing that mass remains singularity-free and shows regular behavior at the core also.

Moving towards, the specific constraint $\frac{2M}{R} < \frac{8}{9}$ suggested by Buchdahl [81] in 1959 for mass and radius relationship is considered. To satisfy this constraint numerically, we find out the value of $\frac{2M}{R}$ for different stars shown in Tables 2–6 which remains consonant with our proposed model.

Moreover, the connection between radius and mass is termed as the compactness and is obtained as:

$$u=\frac{M}{R}. \tag{29}$$

The demeanor of $u(r)$ has been plotted in Fig. 8 (upper right plot) which is increasing and has not crossed the Buchdahl limit. Our model is compatible with another important feature.

4.6. Surface redshift

For the given above compactness $u = \frac{M}{R}$, the surface redshift $Z_s(r)$ for the stellar object is represented as:

$$Z_s=(1-2u)^{-\frac{1}{2}}-1. \tag{30}$$

For the maximum value of surface redshit for a realistic model of a stellar object, many researchers have applied constraints in different conditions (Isotropic, anisotropic, etc.). Such as, for an isotropic matter, this optimal value in the absence of the cosmological constant is 2 [81–83]. Now for anisotropic matter with cosmological constant, according to Bohmer and Harko [84], this value should be $Z_s < 5$ and also in the same criteria, Ivanov [85] suggested the constraint which is $Z_s \leq 5.211$. Now coming towards our proposed model we observed that our model remains consistent with the maximum allowed value as one can see

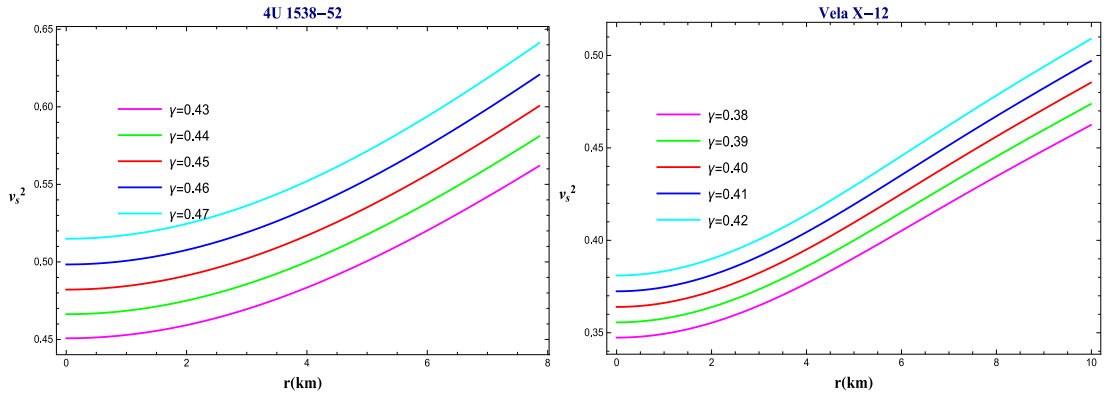

Fig. 7. Graphical representation of the squared sound speed along the radial coordinate illustrating the role of γ. For both the considered stars and for all chosen γ, the value of the squared sound speed remains in the stable region (0,1), as suggested by Herrera.

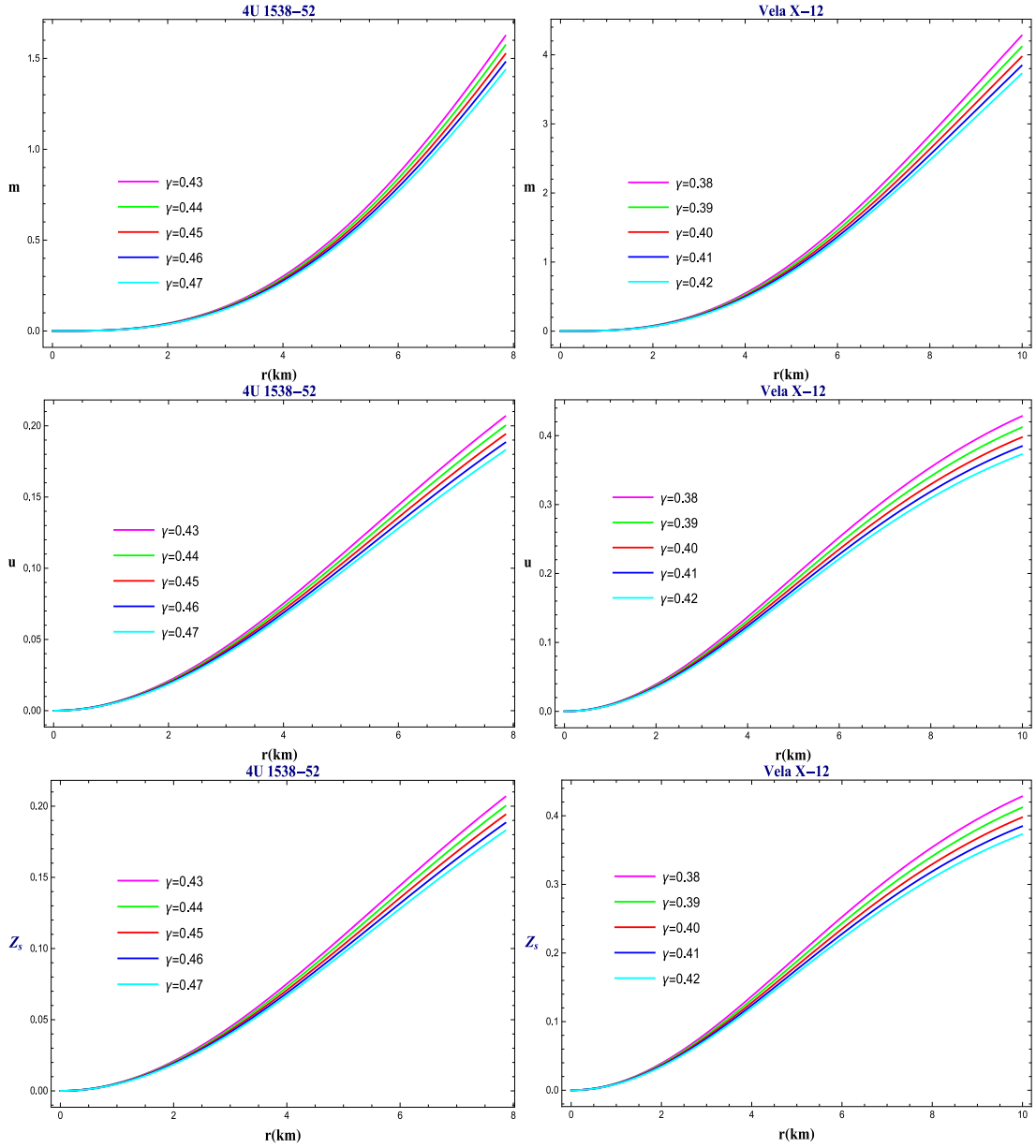

Fig. 8. In this plot, the first row represents the mass function obtained in the current study in the RT along r for two different stars considered in this study and for numerous γ values considered for this study. The conduct increases along the radius and reaches to maximum at the boundary of the star. The second row indicates the graphical illustration of the compactness ($u = \frac{M}{r}$) along the radial coordinate to confirm that the presented model obeys the Buchdahl limit for both the stars and for all curves. The third row demonstrates another important physical requirement, the behavior of the surface redshift and the maximum value of the surface redshift.

graphically in Fig. 8. The numerical values of maximum Z_s for chosen representatives of the compact stellar structure have been shown in Tables 2–7.

5. Conclusions

We construct a new relativistic model of isotropic compact stars in the *RT* by considering the Finch Skea symmetry in the quintessence-like field. For this, we employed the observational data of six different compact stars to verify the physical characteristics of the obtained model. Our model is concurrent with the necessary physical requirements of the realistic model. Some salient traits of the proposed model are discussed in detail in the following points:

- Matter density and pressure: The First feature of our model is that the matter density ρ and the pressure p remain positive throughout the configuration(within the radius) attaining their maximum value at the core as one can see it graphically in Fig. 1 and numerically in Tables 2–6.
- Energy conditions: For the physical plausibility of a model, energy conditions Eq. (25) should be satisfied, and our proposed model is also consistent with all energy conditions (see Fig. 4).
- Dynamical equilibrium of Forces: To check the behavior of different forces acting on our system, we used the TOV equation and observed that for the non-zero value of γ, our system balanced the total effect (Fig. 6) and for $\gamma = 0$ the third force called Rastall force F_r vanishes which shows that the proposed model behaved well according to the conditions.
- Stability analysis: The stability of the model is evaluated through sound speed with the help of casualty condition which suggested that squared sound speed should remain less than the speed of light which is equal to 1 in a realistic unit. We illustrate the V_s graphically and observe that it remains less than 1 which adds more consistency to the proposed model.
- Mass function and Buchdahl Limit: It is necessary for model to be realistic that the mass-to-radius ratio (Compactness) must be regular in the entire configuration, increase towards the surface, and remain zero at the origin. Moreover, the mass function must be non-singular throughout the entire radius. While considering it, we observed that the compactness of our model remains regular, and also mass function remains non-singular throughout the entire radius Fig. 8. In addition, we also satisfy the constraint $\frac{2M}{R} < \frac{8}{9}$ suggested by Buchdahl [81] as one can see in Tables 2–6 for five different stars.
- Surface redshift: In different conditions, different researchers [81–83] suggested different maximum limit values for surface redshift. The proposed model also satisfied the maximum allowed limit value of surface redshift Fig. 8 and also the numerical values of surface redshift are given in Tables 2–6 for different stars.

CRediT authorship contribution statement

M.R. Shahzad: Writing – review & editing, Writing – original draft, Software, Resources, Project administration, Methodology, Investigation, Funding acquisition, Formal analysis, Data curation, Conceptualization. **Asifa Ashraf:** Writing – review & editing, Writing – original draft, Visualization, Validation, Supervision, Software, Investigation, Funding acquisition, Formal analysis, Data curation, Conceptualization. **M. Awais Qarni:** Writing – review & editing, Writing – original draft, Validation, Investigation, Funding acquisition, Formal analysis, Data curation, Conceptualization. **Emad E. Mahmoud:** Writing – review & editing, Writing – original draft, Visualization, Validation, Project administration, Methodology, Data curation, Conceptualization. **Wen-Xiu Ma:** Writing – review & editing, Writing – original draft, Visualization, Validation, Supervision, Formal analysis, Data curation, Conceptualization.

Declaration of competing interest

The authors declare that they have no known competing financial interests or personal relationships that could have appeared to influence the work reported in this paper.

Data availability

Data will be made available on request.

Acknowledgments

The authors extend their appreciation to Taif University, Saudi Arabia, for supporting this work through project number TU-DSPP-2024-94.

References

[1] S. Perlmutter, et al., Supernova cosmology project collaboration, Astrophys. J. 517 (1999) 565.
[2] C.L. Bennett, et al., Astrophys. J. Suppl. 148 (2003) 1.
[3] A.G. Riess, et al., Supernova search team collaboration, Astron. J. 116 (1998) 1009.
[4] P.A.R. Ade, et al., BICEP2 collaboration, Phys. Rev. Lett. 112 (2014) 241101.
[5] W.M. Wood-Vasey, et al., Astrophys. J. 666 (2007) 694.
[6] M. Kowalski, et al., Supernova cosmology project collaboration, Astrophys. J. 686 (2008) 749.
[7] E. Komatsu, et al., WMAP collaboration, Astrophys. J. Suppl. 180 (2009) 330.
[8] M. Tegmark, et al., SDSS collaboration, Phys. Rev. D 69 (2004) 103501.
[9] K. Abazajian, et al., Astron. J. 129 (2005) 1755.
[10] K. Abazajian, et al., SDSS collaboration, Astron. J. 128 (2004) 502.
[11] K. Abazajian, et al., SDSS collaboration, Astron. J. 126 (2003) 2081.
[12] P. Rastall, Phys. Rev. D 6 (1972) 3357A–3360.
[13] N. Dadhich, Gen. Relativity Gravitation 54 (2022) 83.
[14] A. Kusenko, V. Takhistov, M. Yamada, M. Yamazaki, Phys. Lett. B 804 (2020) 135369.
[15] W. Baade, F. Zwicky, Cosmic rays from supernovae, Proc. Natl. Acad. Sci. USA 20 (1934) 254–259.
[16] S.K. Maurya, et al., Eur. Phys. J. C 75 (5) (2015) 225.
[17] S.K. Maurya, et al., Eur. Phys. J. C 84 (3) (2024) 296.
[18] S.K. Maurya, et al., Eur. Phys. J. C 84 (6) (2024) 603.
[19] S.K. Maurya, et al., Fortschr. Phys. 70 (11) (2022) 2200061.
[20] S.V. Lohakare, B. Mishra, S.K. Maurya, K.N. Singh, Phys. Dark Universe 39 (2023) 101164.
[21] S.K. Maurya, Ksh Newton Singh, Abdelghani Errehymy, Eur. Phys. J. Plus 137 (5) (2022) 640.
[22] S. Kaur, S.K. Maurya, S. Shukla, R. Nag, Charged anisotropic fluid sphere in f (R, T) gravity, Chinese J. Phys. 77 (2022) 2854–2870.
[23] A. Ditta, G. Mustafa, S. Maurya, D. SofuoAYlu, A. Mahmood, Classical Quantum Gravity (2024).
[24] N.S. Kavya, G. Mustafa, V. Venkatesha, Ann. Physics (2024) 169723.
[25] J. Bora, D.J. Gogoi, S. Maurya, G. Mustafa, Classical Quantum Gravity (2023).
[26] G. Mustafa, et al., Chinese J. Phys. 88 (2024) 32–54.
[27] A. Ashraf, F. Javed, W.X. Ma, G. Mustafa, Int. J. Geom. Methods Mod. Phys. (2024) 2450161.
[28] G. Mustafa, et al., Chinese J. Phys. 88 (2024) 938–954.
[29] A. Majeed, G. Abbas, M.R. Shahzad, New Astron. 102 (2023) 102039.
[30] G. Abbas, M. Tahir, M.R. Shahzad, Int. J. Geom. Methods Mod. Phys. 18 (03) (2021) 2150042.
[31] M. Tahir, et al., Internat. J. Modern Phys. A 36 (20) (2021) 2150153.
[32] Rabia Saleem, M. Israr Aslam, Shokaib Shahid, Int. J. Geom. Methods Mod. Phys. 21 (05) (2024) 2450106.
[33] K. Majeed, G. Abbas, J. Phys. Commun. 6 (4) (2022) 045005.
[34] H. Moradpour, I.G. Salako, Adv. High Energy Phys. 2016 (2016) 3492796.
[35] H. Moradpour, et al., Accelerated cosmos in a nonextensive setup, Phys. Rev. D 96 (12) (2017) 123504.
[36] J. Fabris, et al., International Journal of Modern Physics: Conference Series, vol. 18, World Scientific Publishing Company, 2012.
[37] F. Darabi, et al., Eur. Phys. J. C 78 (2018).
[38] M. Visser, Phys. Lett. B 782 (2018) 83–86.
[39] S. Hansraj, A. Banerjee, P. Channuie, Impact of the Rastall parameter on perfect fluid spheres, Ann. Phys. 400 (2019) 320.
[40] S. Hansraj, A. Banerjee, Modern Phys. Lett. A 35 (2020) 2050105.
[41] M.R. Shahzad, G. Abbas, Int. J. Geom. Methods Mod. Phys. 9 (2019) 1950132.
[42] M.R. Shahzad, G. Abbas, Eur. Phys. J. Plus 135 (2020) 1–17.
[43] M.R. Shahzad, G. Abbas, Astrophys. Space Sci. 365 (8) (2020) 147.
[44] G. Abbas, M.R. Shahzad, Eur. Phys. J. A 54 (2018) 211.

[45] G. Abbas, M.R. Shahzad, Astrophys. Space Sci. 363 (2018) 251.
[46] G. Abbas, M.R. Shahzad, Astrophys. Space Sci. 364 (2019) 50.
[47] G. Abbas, M.R. Shahzad, Chinese J. Phys. 63 (2020) 1.
[48] H. Nazar, et al., Complexity factor for anisotropic self-gravitating sphere in Rastall gravity, Internat. J. Modern Phys. A 36 (31n32) (2021) 2150233.
[49] Asifa Ashraf, et al., Constraining study of Rastall parameter on charged anisotropic compact star model, Phys. Scr. 98 (3) (2023) 035027.
[50] M. Tahir, G. Abbas, M.R. Shahzad, Instability of gravitating object under expansion-free condition in Rastall theory, Punjab Univ. J. Math. 55 (2023).
[51] G.G.L. Nashed, Nuclear Phys. B 994 (2023) 116305.
[52] A.S. Al-Rawaf, M.O. Taha, Gen. Relativ. Gravity 28 (1996) 935.
[53] C.E.M. Batista, M.H. Daouda, J.C. Fabris, O.F. Piattella, D.C. Rodrigues, Phys. Rev. D 85 (2012) 084008.
[54] T.R.P. Carames, M.H. Daouda, J.C. Fabris, A.M. Oliveira, O.F. Piattella, V. Strokov, Eur. Phys. J. C 74 (2014) 3145.
[55] I.G. Salako, M.J.S. Houndjo, A. Jawad, Internat. J. Modern Phys. D 25 (2016) 1650076.
[56] L.L. Smalley, Phys. Rev. D 9 (1974) 1635.
[57] L.L. Smalley, Phys. Rev. D 12 (1975) 376.
[58] C. Wolf, Phys. Scr. 34 (1986) 193.
[59] T. Manna, F. Rahaman, M. Mondal, Phys. Lett. A 35 (07) (2020) 2050034.
[60] Y. Heydarzade, F. Darabi, Phys. Lett. B 771 (2017) 365A–373.
[61] G.G.L. Nashed, Universe 8 (10) (2022) 510.
[62] G.G.L. Nashed, W.E. Hanafy, Eur. Phys. J. C 82 (8) (2022) 679.
[63] W. El Hanafy, Astrophys. J. 940 (1) (2022) 51.
[64] W. El Hanafy, A. Awad, Astrophys. J. 951 (2) (2023) 144.
[65] W. El Hanafy, Eur. Phys. J. C 84 (4) (2024) 355.
[66] B. Afshar, H. Moradpour, H. Shabani, Phys. Dark Universe 42 (2023) 101357.
[67] B. Dayanandan, et al., Chinese J. Phys. 82 (2023) 155–170.
[68] Michael R. Finch, James E.F. Skea, Classical Quantum Gravity 6 (4) (1989) 467.
[69] Oleksii Sokoliuk, Alexander Baransky, P.K. Sahoo, Chin. Phys. C 47 (1) (2023) 015104.
[70] Shyam Das, et al., Chinese J. Phys. 81 (2023) 362–381.
[71] Bibhash Das, et al., Eur. Phys. J. C 82 (6) (2022) 519.
[72] M. Farasat Shamir, G. Mustafa, Mushtaq Ahmad, Charged anisotropic Finch-Skea-Bardeen spheres, Nuclear Phys. B 967 (2021) 115418.
[73] G. Mustafa, et al., Chinese J. Phys. 88 (2024) 938–954.
[74] S.K. Maurya, et al., Eur. Phys. J. C 82 (12) (2022) 1–15.
[75] Piyali Bhar, et al., Int. J. Geom. Methods Mod. Phys. 18 (10) (2021) 2150160.
[76] M. Sharif, Sana Manzoor, Compact objects admitting Finch-Skea symmetry in f(R, T2) gravity, Ann. Physics 454 (2023) 169337.
[77] P. Rastall, Phys. Rev. D 6 (1972) 3357A–3360.
[78] H. Moradpour, I.G. Salako, Adv. High Energy Phys. 2016 (2016) 3492796, 1A-5.
[79] V.V. Kiselev, Classical Quantum Gravity 20 (2003) 1187.
[80] L. Herrera, Phys. Lett. A 165 (1992) 206A–210.
[81] H.A. Buchdahl, Phys. Rev. 116 (1959) 1027A–1034.
[82] N. Straumann, Springer Verlag, Berlin, 1984.
[83] C.G. Bohmer, T. Harko, Gen. Relativity Gravitation 39 (2007) 757A–775.
[84] C.G. Bohmer, T. Harko, Classical Quantum Gravity 23 (2006) 6479A–6491.
[85] B.V. Ivanov, Phys. Rev. D 65 (2002) 1A–17, 104001.